Applied Catalysis B: Environmental 198 (2016) 112–123

Contents lists available at ScienceDirect

Applied Catalysis B: Environmental

journal homepage: www.elsevier.com/locate/apcatb

MIL-53(Fe)-graphene nanocomposites: Efficient visible-light photocatalysts for the selective oxidation of alcohols

Zhiwang Yang*, Xueqing Xu, Xixi Liang, Cheng Lei, Yuli Wei, Peiqi He, Bolin Lv, Hengchang Ma, Ziqiang Lei*

Key Laboratory of Polymer Materials of Gansu Province, Key Laboratory of Eco-Environment-Related Polymer Materials, Ministry of Education, College of Chemistry and Chemical Engineering, Northwest Normal University, Lanzhou 730070, China

ARTICLE INFO

Article history:
Received 20 April 2016
Received in revised form 10 May 2016
Accepted 20 May 2016
Available online 20 May 2016

Keywords:
MIL-53(Fe)
Graphene
Visible light photocatalysis
Direct hole oxidation
Alcohol oxidation

ABSTRACT

A series of MIL-53(Fe)-graphene nanocomposite photocatalysts were synthesized by a facile one-pot solvothermal reaction. All materials have been thoroughly characterized by FT-IR, SEM, TEM, PXRD, UV–vis DRS and PL analysis. It was demonstrated that the introducing of graphene on the MIL-53(Fe) would minimize the recombination of photogenerated electron-hole pairs, thus, leading to the enhancement of photocatalytic activity. MIL-53(Fe)-graphene nanocomposite was an efficient catalyst towards the photocatalytic selectively oxidation of alcohols to the corresponding aldehydes or ketones under visible light and ambient conditions. High selectivity of the aldehydes or ketones (99%) were obtained. Meanwhile, the catalyst can be recycled at least four times without loss of catalytic efficiency. A possible photocatalytic reaction mechanism involving a direct photogenerated hole-oxidation process was also investigated in detail by the active species trapping experiments and the related electrochemical analysis.

1. Introduction

Metal-organic frameworks (MOFs), an interesting class of multifunctional inorganic-organic hybrid diverse porous and functionalized 3D crystalline materials, have shown potential applications in many field including gas storage, luminescent properties, magnetic materials, separation, chemical sensing, drug delivery etc [1–5]. Especially, MOFs are used for the development of heterogeneous catalysts. In fact, a variety of heterogeneous MOF-based catalysts has been realized over the past decades by introducing different types of catalytic sites into a porous MOFs matrix [6,7].

Photocatalysis is a unique kind of heterogeneous catalysis which involves the use of light source. Theoretically, it is also feasible to develop MOFs-based photocatalysts by immobilizing photoactive catalytic sites to MOF materials [8]. T. Tachikawa and his colleagues have revealed that MOF-5 can behave as a semiconductor upon light excitation [9]. After that, an increasing number of papers have appeared in the literatures to indicate that MOFs provide a unique opportunity for integrating different molecular functional components to the photocatalytic hydrogen evolution [10,11], CO_2 reduction [12–15], degradation of organic dye [16] and organic transformations [17,18]. All these studies demonstrated that MOFs have high potential as promising photocatalysts in the future. Hereinto, photocatalysis for selective organic transformations have gained extensive attentions due to its mild, clean, and atom-efficient methodologies for organic synthesis [19].

Among the diverse photocatalysts, Fe-based MOFs were aroused extremely interest, since iron is an earth-abundant element and iron-containing complexes are commonly used in catalysis and photocatalysis [20]. Besides, It is worth mentioning that almost all of the Fe-based MOF materials already reported are visible-light-responsive due to the existence of extensive iron oxo clusters [21–23]. In particular, MIL-53(Fe) is a three-dimensional porous solids composed of infinite $FeO_4(OH)_2$ cluster connected by 1,4-benzenedicarboxylate (H_2BDC) ligand [24–26]. It is a visible-light-responsive photocatalyst for the degradation of organic dye [20] and CO_2 reduction [16]. In this study, photocatalysis for selective organic transformations by MIL-53(Fe) was focused. To further improve the photocatalytic performances of MIL-53(Fe), some researchers have attempted their efforts on the introduction of functional entities into such materials.

Graphene (GR) [27], as a new type of carbon materials with unique 2D structure and high electron conductivity, has been projected as a rising star in the field of materials science. More recently,

* Corresponding author.
E-mail addresses: yangzw@nwnu.edu.cn, yangzw_nwnu@163.com (Z. Yang), leizq@nwnu.edu.cn (Z. Lei).

http://dx.doi.org/10.1016/j.apcatb.2016.05.041
0926-3373/

graphene has also been regarded as a kind of ideal functional material for photocatalyst carrier and promoter to accept and shuttle electrons photogenerated from semiconductors upon light irradiation, thus enhancing the photoactivity of semiconductors [28–30]. Naturally, a lot of efforts were directed to the preparation of GR-MOFs composites for the improvement of the photocatalytic efficiency of the MOFs [31–33].

However, classical and modified Hummer's methods about the preparation of the GR need complicated process and long time [34]. In this paper, a solution-based oxidative process reported by the D V. Kosynkin and his colleagues [35] was accept to prepared the graphene from the multi-walled carbon nanotubes (MWCNTs). We primarily focus on the fabrication of MIL-53(Fe)-graphene (M53/GR) nanocomposites and, specifically their application in the selective oxidation of alcohols. Moreover, as we might expect, introducing graphene into the MIL-53(Fe) could improve the photocatalytic activity by facilitating the transfer of photogenerated charge and reducing the recombination of photogenerated electron-hole pairs.

Selective oxidation of alcohols, recognized as one of the most fundamental transformations in organic synthesis, has provided the main breakthrough instead of traditional environmentally undesired stoichiometric oxidation systems. What is more, photocatalytic aerobic oxidation of alcohols into carbonyl compounds using molecular oxygen in the presence of photocatalyst has attracted much attention because of the advantage of using O_2 as a green oxidant and light as the reaction driving force [36]. Besides, it is also generally accepted that photogenerated holes with possible strong oxidation capacity to oxidize the benzyl alcohol directly. Moreover, the selectivity of photocatalytic oxidation of benzyl alcohol is highly depended on the position of valence band of semiconductors [37].

View of that, the selective oxidation of alcohols by the photogenerated holes has aroused our attention. Form the experiment result, we luckily found that the flat band potential of M53/GR is about −0.38 V *vs* SCE (equivalent to −0.14 V *vs* NHE). Accordingly, the conduction band potential (E_{CB}) of M53/GR is determined to be −0.24 V *vs* NHE and the valence band potentials (E_{VB}) of M53/GR is calculated to be 2.09 V *vs* NHE. It is more positive than the reduction potentials of benzyl alcohol/benzaldehyde (1.88 V), but less positive than that of benzaldehyde/oxidized benzaldehyde (2.77 V). So it is worth mentioning that M53/GR is thermodynamically permissible photocatalyst for the selective oxidation of alcohols to the corresponding or ketones using photogenerated hole (h^+) as the oxidant rather than O_2. At the same time, aldehydes or ketones can not be further oxidized. Thus, the selectivity of the aldehydes or ketones was improved significantly. Therefore, direct hole oxidation process would be used as a potential and promising strategy for the selective oxidation of alcohols.

2. Experimental

2.1. Materials

All the used reagents and solvents were analytical grade and used as received from commercial sources without further purification. 1,4-Benzenedicarboxylic acid (H_2BDC), benzyl alcohol, 4-methoxybenzyl alcohol were obtained from Aladdin Reagent Co. Ltd. Iron(III) chloride hexahydrate, ethanol, sulfuric acid (98%), *N*,*N*-dimethylformamide (DMF), tetrachloromethane, hydrogen peroxide (30%), and potassium permanganate were supplied from Sinopharm Chemical Reagent Co. Ltd. Multi-walled carbon nanotubes (MWCNTs) with outside diameters of 30–50 nm, lengths of 10–20 um was purchased from Times Nano Company of Chengdu Organic Chemistry Co. Ltd. 4-Nitrobenzyl alcohol, 2-methylbenzyl alcohol, 4-chlorobenzyl alcohol, 2-methoxybenzyl alcohol, 4-hydroxybenzyl alcohol, benzhydrol, 4-chlorobenzhydrol and 4-methoxybenzhydrol were obtained from the Beijing J&K Scientific Co. Ltd. 4-Methylbenzyl alcohol, 4, 4′-dimethylbenzhydrol, 4, 4′-dimethoxylbenzhydrol and 4, 4′-dichlorobenzhydrol were obtained from Alfa Aesar Co. Ltd.

2.2. Preparation of photocatalysts

2.2.1. Synthesis of MIL-53(Fe)

MIL-53(Fe) was synthesized according to the literature [14]. In a typical procedure, a mixture of $FeCl_3{\cdot}6H_2O$ (0.674 g), H_2BDC (0.415 g), and 56 mL of DMF (with the molar ratio of 1:1:280) were stirred at room temperature until it become a clear solution, then it was transferred into a 100 mL Teflon liner. After that, the Teflon liner was sealed in a stainless steel autoclave and heated at 170 °C for 24 h. The resultant suspension was filtered, washed with DMF and C_2H_5OH, respectively. The yellow powder was collected by filtering and drying under vacuum at 100 °C for 10 h.

2.2.2. Synthesis of graphene oxide nanoribbons

Graphene nanoribbons were synthesized by the method from D. V. Kosynkin's report [35]. Typically, 2.0 g of MWCNTs was dispersed in 60 mL of concentrated sulphuric acid and continuously stirred for 6 h at room temperature. 10.0 g of $KMnO_4$ was added and the mixture allowed to stir for 2 h at room temperature, then heated in an oil bath at 70 °C with stirring for another 6 h. The suspension was cooled down to room temperature, and the reaction was quenched by a small amount of hydrogen peroxide. The solution was filtered and the residual was washed with diluted hydrochloric acid solution and redistilled water several times until the pH value of the filtered liquid reached about 7, then the solid was dried under vacuum at 60 °C for 24 h and the target product, graphene oxide nanoribbons (GO) was obtained.

2.2.3. Synthesis of M53/GR nanocomposites

A series of MIL-53(Fe)-graphene nanocomposites with different mass ratios of MIL-53(Fe) *vs* graphene were synthesized by a facile one-pot solvothermal reaction. Firstly, a certain amount of GO power was dispersed into 10 mL of DMF with the aid of ultrasonication for 120 min. Then a mixture of $FeCl_3{\cdot}6H_2O$ (0.674 g), H_2BDC (0.415 g), 56 mL of DMF were stirred at room temperature, when it became a clear solution, the GO/DMF mixture (10 mL) was added into the above solution with continuously stirring for another 1 h. Then it was subjected to solvothermal conditions in a Teflon-lined stainless steel autoclave for 24 h at 170 °C. Besides, this solvothermal process was used to reduction of GO to GR [31]. The autoclave was cooled naturally to room temperature, and the resultant precipitate was separated by centrifugation, washed repeatedly with DMF and C_2H_5OH. Finally, the samples were dried at 100 °C under vacuum. The final products were labeled as M53/GR-4, M53/GR-8, and M53/GR-12 (the numbers in the abbreviated name on behalf of the weight content of the GR for 0.4%, 0.8%, and 1.2%, respectively).

2.3. Instrumental

The Fourier transform-infrared spectroscopy (FT-IR) was carried on a Nicolet NEXUS 670 spectrometer using KBr disks in the scanning range of 4000–400 cm^{-1}. The powder X-ray diffraction (XRD) were carried on a Rigaku D/Max-2400 diffractometer with Cu Kα radiation (k = 1.5418 Å). UV–vis diffuse reflectance spectra (UV–vis DRS) wasobtained by a Cary 500 UV–vis-NIR spectrophotometer. The photoluminescence spectra (PL) was conducted on a PELS-55 Luminescence Fluorescence Spectrophotometer. The morphology of the samples was characterized by field emission scanning electron microscopy (FE-SEM, Ultra Plus, Carl Zeiss, Germany).

Transmission electron microscopy (TEM) was measured using a JEOL model JEM2010 EX microscope at an accelerating voltage of 200 kV. The XPS analysis (ThermoVG Scientific Sigma Probe) with an Al Kα radiation was used to study the surface compositions of the catalysts. The electrochemical analysis including Mott-Schottky analysis, electrochemical impedance spectroscopy (EIS) and the cyclic voltammetry (CV) of benzyl alcohol and benzaldehyde were performed on an electrochemical workstation (CHI660B, Shanghai, Inc.). The products of the selective oxidation of alcohols were recorded through gas chromatograph (GC) analyses on a Shimadzu GC-2010 equipped with an RTX-1 capillary column and an FID detector.

2.4. Photocatalytic experimental details

In the photocatalytic activity text, aryl alcohol (0.3 mmol) was dissolved in a solution of 10 mL of CCl_4 in the presence of 15 mg catalyst in an open quartz tube and the suspension was stirred in the dark for 1 h to ensure the establishment of adsorption-desorption equilibrium. The solution was then irradiated under a visible-light illumination. A 500 W Xe lamp (λ > 400 nm) (PLS-SXE 300, BiLon Co. Ltd., Shanghai China) with a 400 nm cutoff filter was used as the visible-light source. Then the reaction mixture was irradiated for appropriate time under room temperature. After reaction, the reaction conversion and the assignment of products were recorded on a gas spectrometry. A standard curves using toluene as internal standard was adopted to calculate the conversion of alcohol and selectivity for aldehyde or ketone. The conversion of alcohol and the selectivity of aldehyde or ketone in the reaction process could be calculated by the Formulas (1) and (2), respectively.

$$\text{Conversion of the alcohol } \% = \frac{C_0 - C_n}{C_0} \times 100\% \quad (1)$$

$$\text{Selectivity of the aldehyde } \% = \frac{C_a}{C_0 - C_n} \times 100\% \quad (2)$$

where C_0 is the initial concentration of alcohol prior to reaction, C_n and C_a is the concentration of alc ohol and aldehyde measured at the time *t*. respectively.

2.5. Electrochemical measurements

The Mott-Schottky measurements to evaluate the band positions of the M53/GR, were carried out with AC impedance-potential model in a standard three-electrode system, namely, a saturated calomel electrode (SCE) as a reference electrode, a Pt foil as the counter electrode, and M53/GR as the working electrodes. The M53/GR electrodes were prepared according to Zhang's method [38]. For the preparation of composite electrodes, MIL-53(Fe)/GR composites were dispersed in chitosan solution to form a 5 mg·mL^{-1} solution and ultrasonicated for 30 min, then 0.2 mL of colloidal solution was dropped on the conductive side of the FTO glass and allowed to dry for 12 h at room temperature in the air.

Electrochemical impedance spectroscopy (EIS) tests were performed under dark condition at open circuit potential over the frequency range between 10^5 and 10^{-2} Hz, with an AC voltage magnitude of 5 mV. All of the measurements were performed in 0.5 M Na_2SO_4 solution.

The cyclic voltammetry (CV) was measured by sweeping at 0.05 V/s in 0.5 M Na_2SO_4/*x* mmol L^{-1} benzyl alcohol and 0.5 M Na_2SO_4/*x* mmol L^{-1} benzaldehyde (*x* = 0.1, 0.3 and 0.5). A glass carbon disk, a Pt foil and an SCE were used as the working, counter and the reference electrodes, respectively. The redox potentials of benzyl alcohol and benzaldehyde were evaluated from the results of voltammogram analysis.

3. Results and discussion

3.1. Characterization

The crystallographic structure of the as-prepared MIL-53(Fe) and a series of M53/GR nanocomposites were examined by powder X-ray diffraction (PXRD) (Fig. 1a). Apparently, the well-defined diffraction peaks revealed the high crystallinity of the MIL-53(Fe) were consistent with the simulated one [39]. Moreover, the samples of M53/GR-4 and M53/GR-8 exhibit the similar XRD patterns as that of the MIL-53(Fe), implying that the introduction of GR has no effect on the crystal structure of MIL-53(Fe) [38]. On account of the low amount of GR in the M53/GR, the characteristic diffractions for GR were not being observed in the M53/GR-4 and M53/GR-8 nanocomposites. However, when continuing to increase the content of the GR, the signals of these peaks emerged slightly, indicating that after the excess introduction of GR, the crystallinity of the MIL-53 changed due to the dispersed of GR on the surface of MIL-53.

In order to further identify the functional groups and analyze the molecular structure of M53/GR samples, the FT-IR spectroscopy of MIL-53(Fe), and different M53/GR composites were performed and the results were shown in Fig. 1b. Characteristic absorption peaks of the MIL-53(Fe) samples were observed at 1649, 1526, 1382, 1023, and 745 cm^{-1}, these are identical to those of reported data in the literatures [40]. The absorption peaks of C=O stretching mode can be observed at 1629 cm^{-1}. The two intense peaks at 1526 and 1387 cm^{-1} correspond to asymmetric and symmetric vibrations of carboxyl groups, respectively. These results confirm the presence of the dicarboxylate linker within frameworks. The peak at 745 cm^{-1} corresponds to C—H bending vibrations of the benzene in the organic linkers. Besides, well matched spectra with MIL-53(Fe) can be observed on these M53/GR composites. Therefore, the results of XRD analysis and FT-IR spectra clearly confirm the formation of MIL-53(Fe) structure.

The morphology of the MIL-53(Fe) and M53/GR were characterized by SEM and TEM showed in Fig. 2. The original MIL-53(Fe) shows the polyhedron structure with lengths of 2 μm and smooth surfaces (Fig. 2a). From the SEM images of M53/GR, moreover, it can be seen that the nanocomposite maintains the polyhedron structure of the MIL-53(Fe), and GR spread densely and tightly on the surface of MIL-53(Fe), resulting in a rough surface of the nanocomposite. It could be due to the "GO-structure-directing" growth of MIL-53(Fe) on the GR sheets during an in situ wet chemistry process (Fig. 2b) [41]. The TEM image of the M53/GR (Fig. 2c) further confirmed this conclusion, where the GR nanolayers wrapped closely on the surface of MIL-53(Fe). Moreover, the TEM image shown the GR was well-crystallized (Fig. 2d), and the sharp edges made by perfect graphitic layer with a (002) crystal plane corresponding to a *d* spacing about 0.35 nm appeared clearly, which is closer to that of single-crystal graphite (0.335 nm) [42].

The elemental composition and electronic structure of M53/GR composite was analyzed by X-ray photoelectron spectroscopy (XPS). XPS survey spectrum (Fig. 3a) demonstrates that C, O and Fe elements existed in the M53/GR. The high-resolution XPS spectrum (Fig. 3b) of C 1 s can be deconvoluted into three surface components at 284.6, 285.6 and 288.6 eV. The peak at 284.6 eV corresponds to sp^2 carbon in GR and benzoic rings [43]. The peak at 285.6 eV of C—C mainly resulted from the GR. The carboxylate groups (C=O) of H_2BDC linkers is at the binding energy of 288.6 eV [44]. For the Fe 2p spectrum (Fig. 3c), the binding energy peak at 712.0 is ascribed to the Fe $2p_{3/2}$, and the peak at 725.7 eV is assigned to the Fe $2p_{1/2}$ [45]. The peak separation, namely, $\Delta = 2p_{1/2}\text{-}2p_{3/2} = 13.7$ eV, is very similar to those reported for α-Fe_2O_3 [46]. In addition, the peak associated with shake up lines for metal transitions at 715.8 eV was also observed [47]. The above results are the characteristic

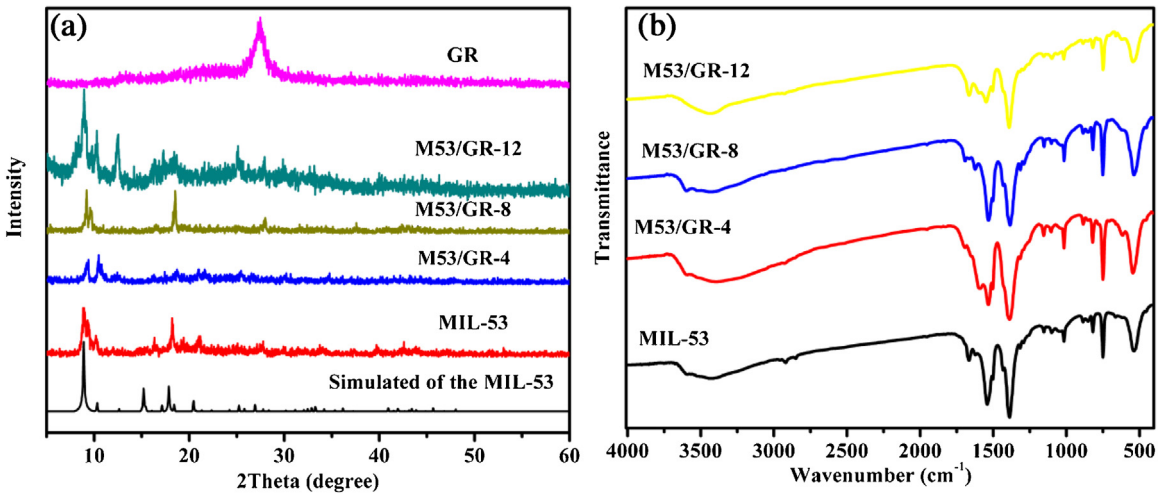

Fig. 1. The PXRD patterns (a) and the FT-IR spectroscopy (b) of the samples.

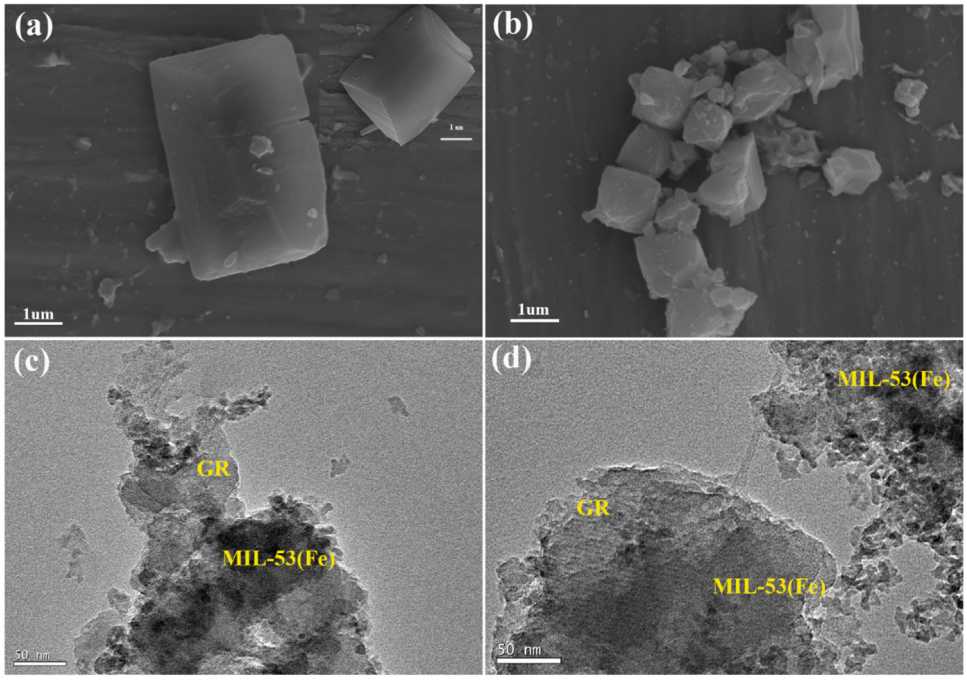

Fig. 2. SEM images of MIL-53(Fe)(a) and M53/GR-8 (b), TEM images of the M53/GR-8 (c and d).

of Fe^{3+} in MIL-53(Fe) structure. Fig. 3d shows the high-resolution XPS spectra of O 1s, fitted by two peaks at binding energies of 531.5 eV and 532.3 eV, which are attributed to the oxygen atoms in the carboxylate groups of the H_2BDC linkers and the Fe-O bonds of MIL-53(Fe), respectively [38]. These results are all consistent with that of the FT-IR spectra and further confirm the conformation of M53/GR composites.

The absorbance properties of the as-prepared samples were measured using UV–vis diffuse reflection spectroscopy (UV–vis DRS). As shown in Fig. 4a, all of the samples show the strong absorption bands at the range of 200–460 nm. For the MIL-53, the characteristic absorption signal was observed at about 250 nm, which can be assigned to the absorption induced by ligand-to-metal charge transfer (LMCT) of O(II) to Fe(III) [9]. Moreover, the small peak centered at 445 nm may be due to the transition ($^6A_{1g} => {}^4A_{1g} + {}^4E_g(G)$) in Fe (III) [48]. Clearly, the onset of the main absorption edge of MIL-53(Fe) was located at 456 nm. Based on the relation of $E_g = 1240/\lambda$ [49], the calculated optical bandgap of MIL-53(Fe) was 2.72 eV. After GR is wrapped on the surface of MIL-53, the absorption of M53/GR composites was enhanced, distinctly in the visible light zone. Especially, the optical bandgap of M53/GR-8 is 2.33 eV. As expected, the optical properties of M53/GR could contribute to possessing efficient photo reactivity at visible light region.

The photoluminescence (PL) spectra clarified the efficient separation of the photoexcited electron-hole pairs of M53/GR. For MIL-53(Fe), a broad band at 340–540 nm with a peak at 430 nm was detected, which is attributed to the 1, 4-benzenedicarboxylic acid linkers in MIL-53(Fe) structure [20]. The similar peaks were presented in the M53/GR nanocomposites. It can also be found that the PL intensity of the photocatalyst followed the order: MIL-53(Fe) > M53/GR-4 > M53/GR-12 > M53/GR-8, indicating that the M53/GR-8 has the longest lifetime of electron-hole pairs. Combined with the conclusion of the SEM and TEM, it was confirmed that the intimate interfacial contact between the MIL-53(Fe) and

Table 1
Photooxidation of various substituted benzyl alcohols over M53/GR catalyst.

[a]Entry	Substrate	Product	[b]Con./%	[c]Sel./%
1	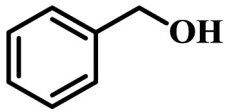	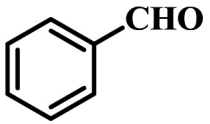	80	100
2	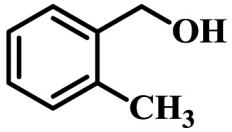	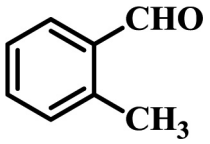	83	100
3	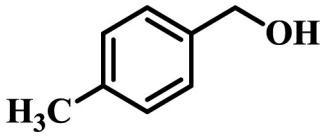	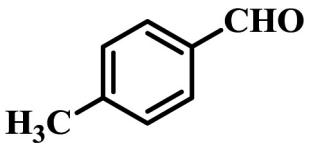	84	100
4	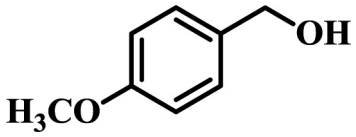	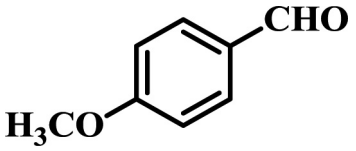	85	100
5	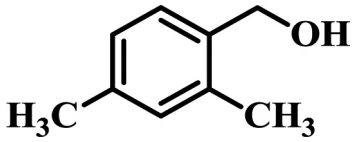	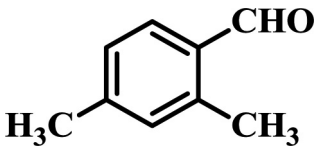	87	100
6	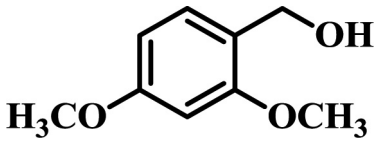	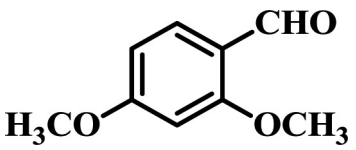	87	100

Table 1 (*Continued*)

[a]Entry	Substrate	Product	[b]Con./%	[c]Sel./%
7	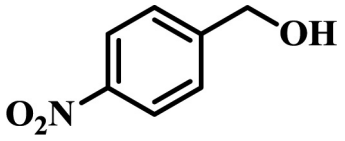	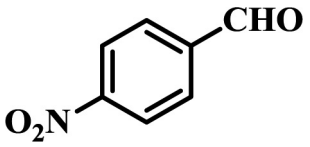	74	100
8	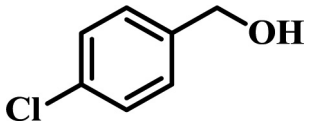	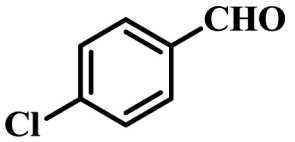	76	100
9	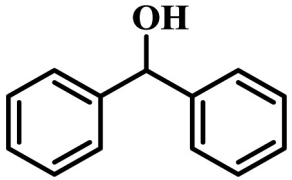	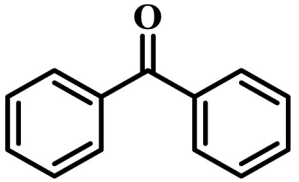	56	100
10	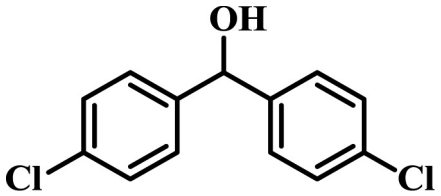	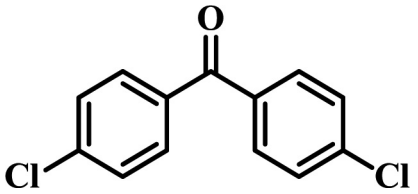	44	100
11	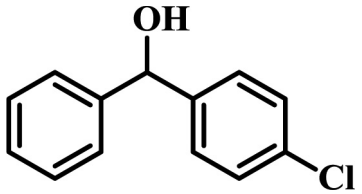	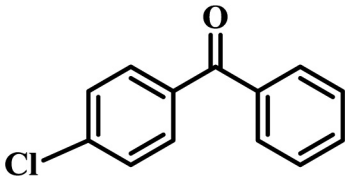	48	100

Table 1 (*Continued*)

[a]Entry	Substrate	Product	[b]Con./%	[c]Sel./%
12	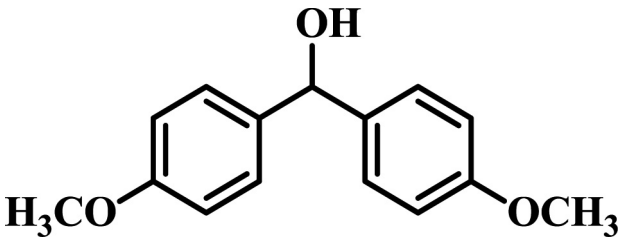	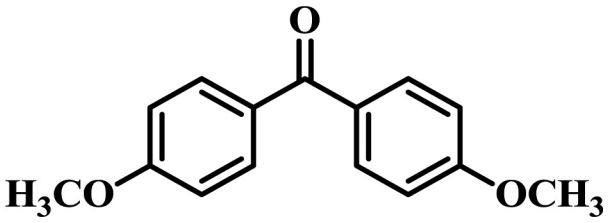	68	100
13	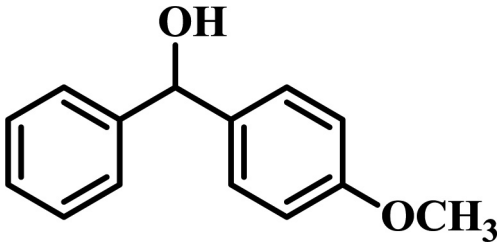	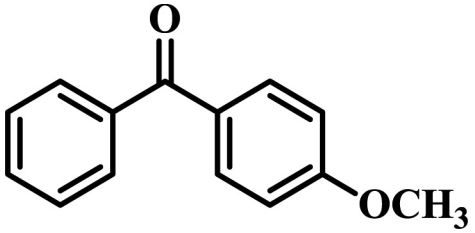	64	100
14	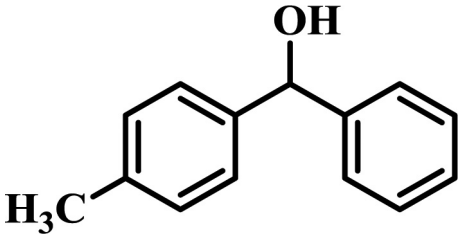	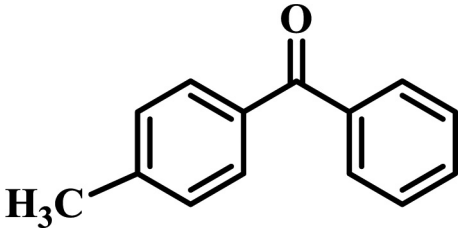	58	100
15	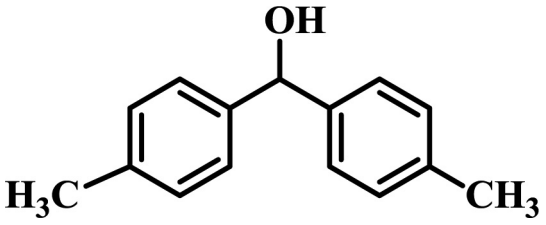	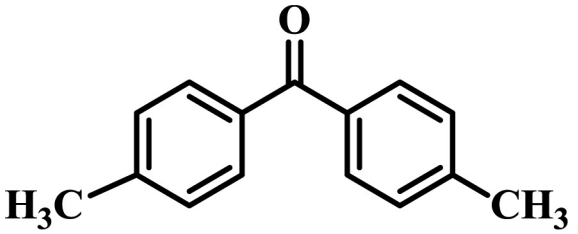	58	100

[a] Reaction conditions: aryl alcohols 0.3 mmol, CCl_4 10 mL, M53/GR-8 15 mg 9 h, visible-light illumination under ambient conditions.
[b] Calculated by GC analysis.
[c] Selectivity for aromatic aldehydes.

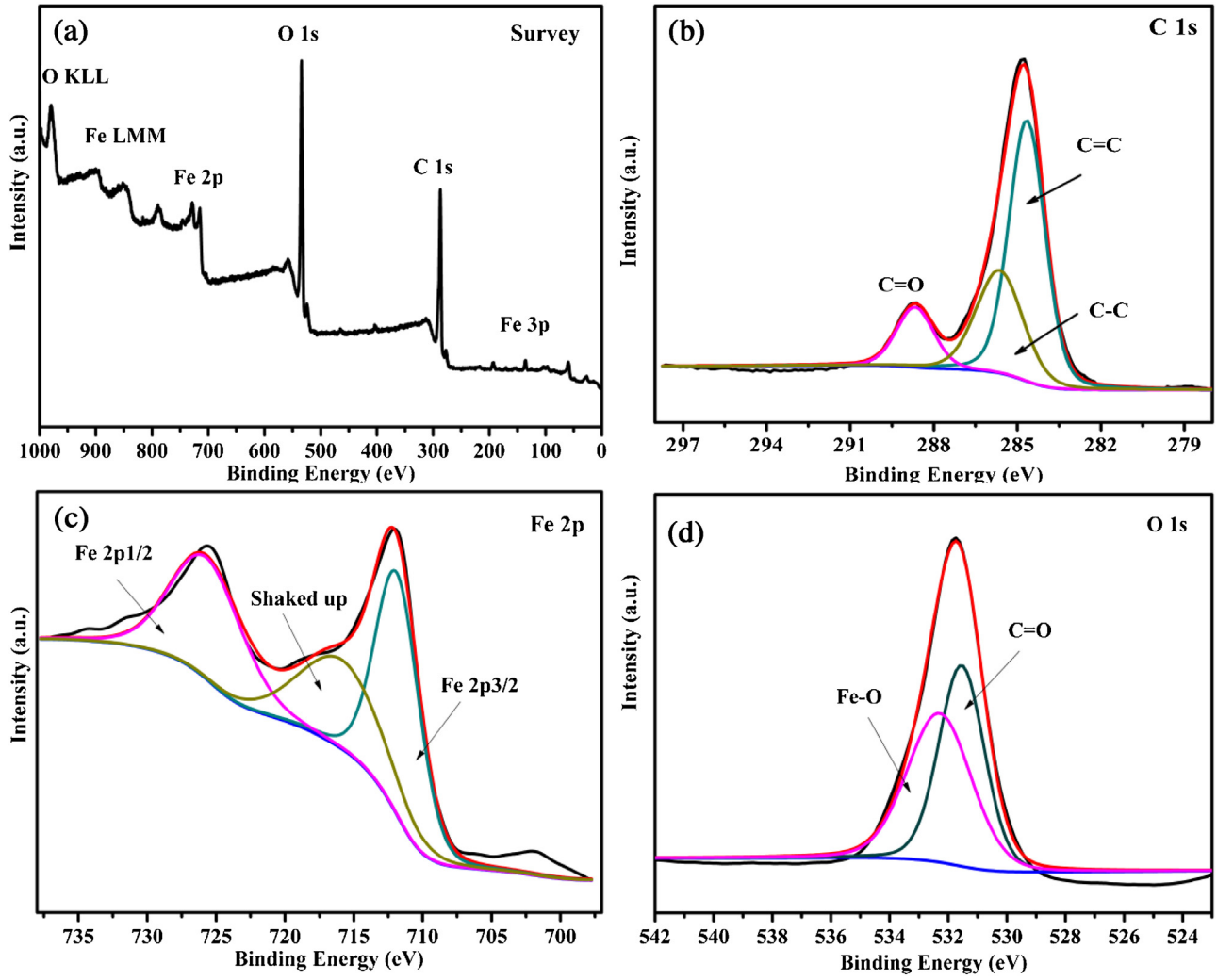

Fig. 3. The XPS survey spectrum and deconvoluted XPS of the M53/GR-8. Typical wide survey (a), and high resolution XPS spectrum of C 1 s (b); Fe 2p (c); O 1 s (d). Black line is the obtained chart, and red line is the sum of the deconvoluted components. (For interpretation of the references to colour in this figure legend, the reader is referred to the web version of this article.).

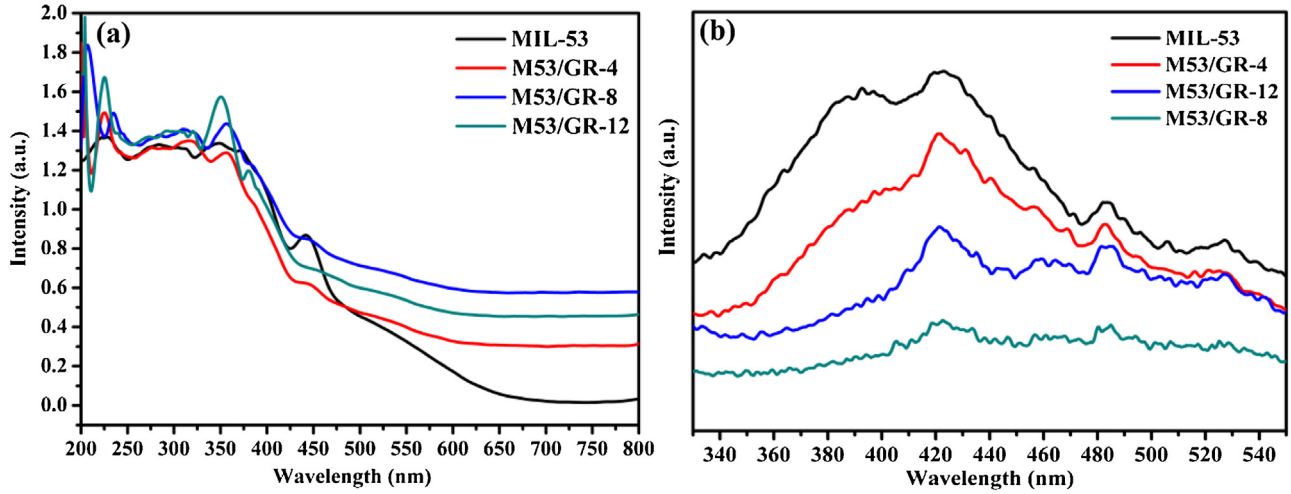

Fig. 4. UV–vis diffuse reflectance spectra (UV–vis DRS) (a) and photoluminescence spectra (PL) (b) of the samples.

the GR could improve the photon-generated carrier transfer, in other word, GR can act as a good acceptor for the photogenerated electrons, and consequently, the recombination of the photo electron-hole is inhibited. This long-lived charge separated state would make the M53/GR more efficient for photocatalytic applications.

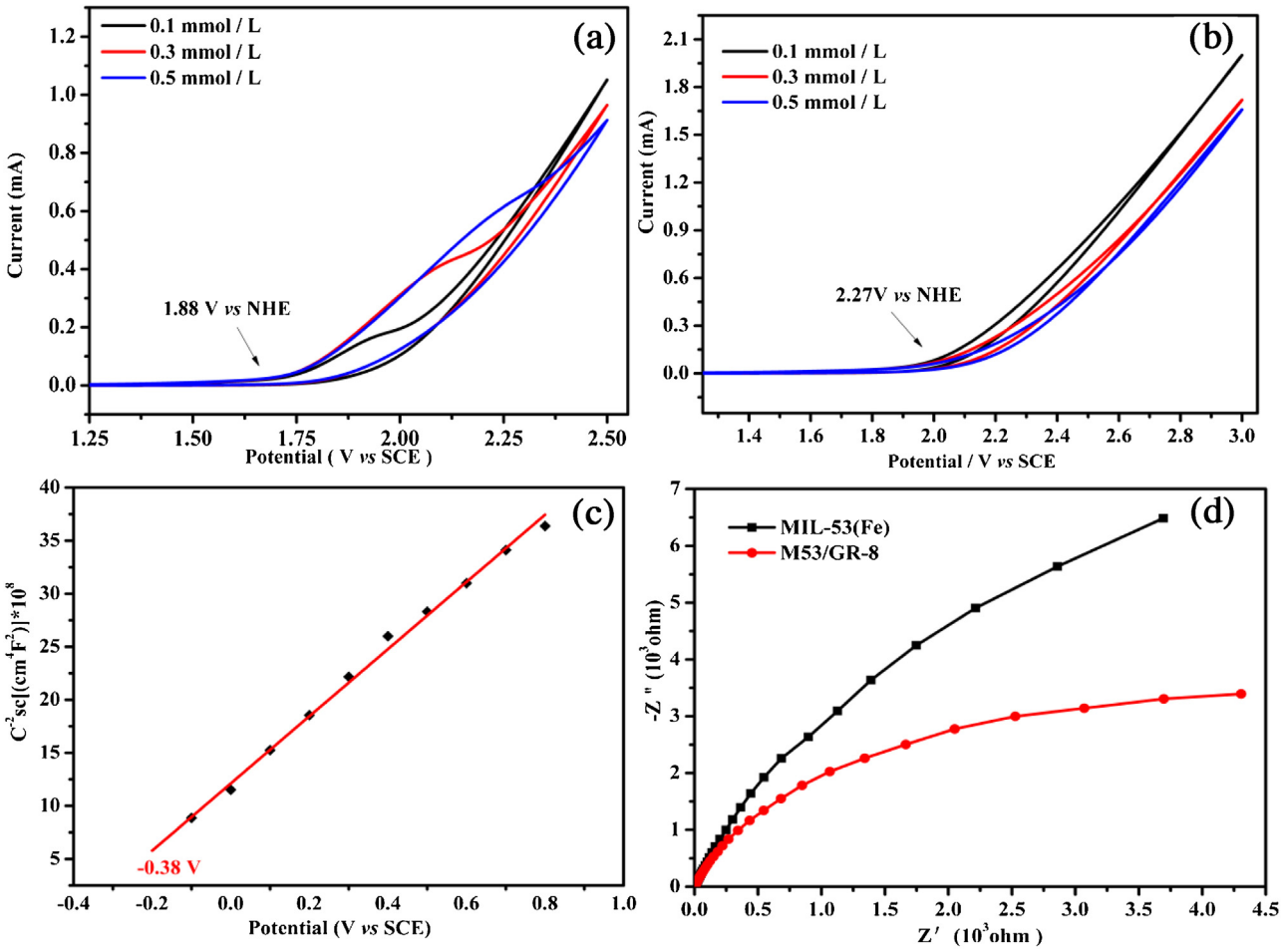

Fig. 5. The electrochemical analysis of the samples. The cyclic voltammogram of benzyl alcohol (a) and benzaldehyde (b); Mott-Schottky plot for the M53/GR electrodes (c); EIS Nyquist plots of bare MIL-53(Fe) and M53/GR-8 composites under dark condition (d).

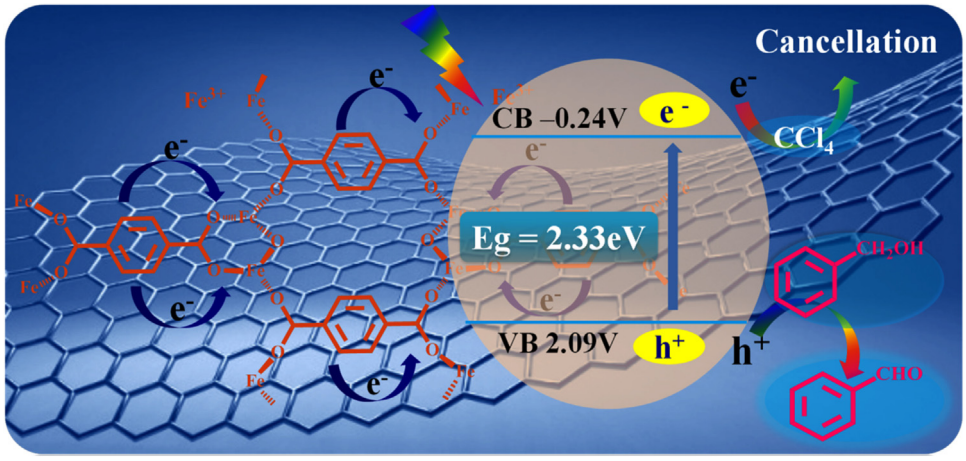

Scheme 1. The proposed mechanism for photocatalytic oxidation of the benzyl alcohol by the M53/GR.

3.2. Photocatalytic activity

To investigate the scope of this catalytic system, the catalytic activity of the M53/GR has been assessed to studying the photooxidation of various substituted benzyl alcohols. As seen in Table 1, many of the benzyl alcohols were oxidized to the corresponding aryl aldehydes or ketone within 9 h irradiation. Notably, all the oxidations selectivity to the corresponding aldehydes is nearly 100%. Primary benzylic alcohols possessing electron-donating substituents such as methyl and methoxy on the aromatic ring were oxidized to the corresponding aldehydes with higher conversions in all of the series (**Entries 1–6**). On the contrary, due to the electron-withdrawing ability, alcohols with the nitro and chlorine on the aromatic ring have the lower conversions (**Entries 7–8**). In all of the oxidations, secondary benzylic substrates had lower conversions (**Entries 9–14**) compared that of the primary benzylic

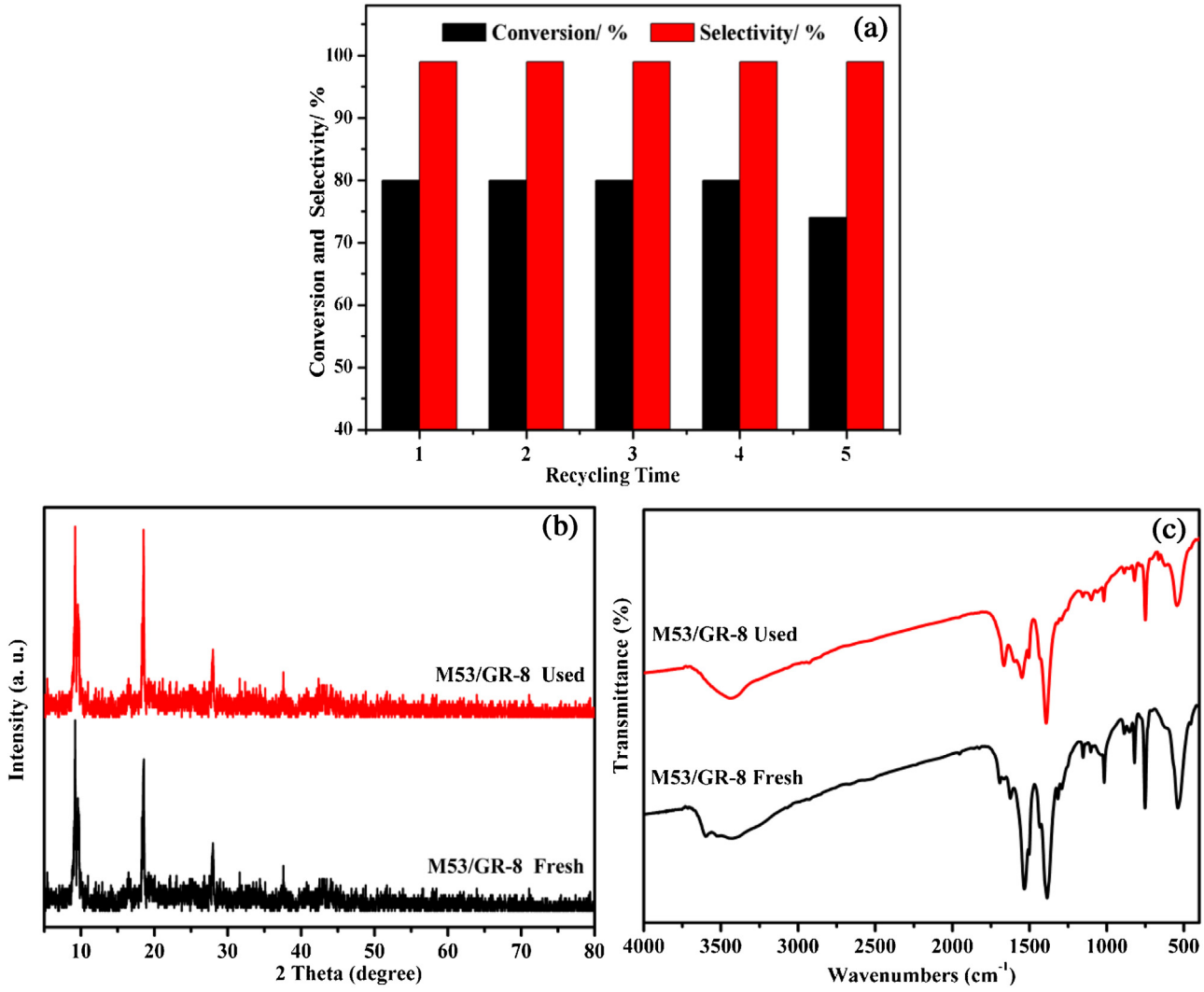

Fig. 6. The cycling runs of the oxidation of the benzyl alcohol over M53/GR system (a); PXRD patterns (b); and FT-IR spectra (c) of M53/GR before and after catalytic reaction.

alcohols. It might attribute to the larger steric hindrance of the aryl groups. Besides, the electronic effect observed from the primary benzylic systems also seems to be prevalent in the case of benzohydrol systems. For example, the existing of a chlorine group (**Entries 10 and 11**) resulted in a lower conversion than that of the electron-rich ones (**Entries 12–15**).

3.3. *Mechanism for the photooxidation of benzyl alcohol over M53/GR*

To further study the possible mechanism for the photooxidation of benzyl alcohol over M53/GR, we carried out the blank control and active species trapping experiments and electrochemical technique including Mott-Schottky experiments and cyclic voltammetry (CV) evaluation of benzyl alcohol and benzaldehyde.

The redox potentials of benzyl alcohol and benzaldehyde with different concentrations (0.1, 0.3, and 0.5 mmol L^{-1}) were evaluated using cyclic voltammetry, respectively. It was found that the reduction potentials of benzyl alcohol/benzaldehyde and benzaldehyde/oxidized benzaldehyde were independent on the concentrations. It was calculated that the potentials of benzyl alcohol and benzaldehyde are 1.88 and 2.27 V, respectively (Fig. 5a and b). To better clarify the electronic properties of M53/GR, Mott-Sckottky measurements have been carried out. As displayed in Fig. 5c, the slope of linear $1/C^2$ potential curve was positive, indicating that M53/GR-8 is an n-typed semiconductor [50]. The calculated flat-band potential of M53/GR is -0.38 V *vs* SCE at pH 7.0, corresponding to ca. −0.14 V *vs* NHE. For many n-typed semiconductor, the conduction band potential is more negative about 0.1 V for the flat-band potential [51], so the conduction band potential (E_{CB}) of the M53/GR is -0.24 V *vs* NHE. Combining with the band gap energy estimated from UV–vis DRS spectra, the calculated optical bandgap of M53/GR is 2.33 eV. Accordingly to the empirical formula of $Eg = E_{VB} - E_{CB}$, the valence band position (E_{VB}) of M53/GR is determined to be 2.09 V *vs* NHE, which is more positive than the potential of benzyl alcohol (1.88 V *vs* NHE), and it is inferior to the potential of benzaldehyde (2.27 V *vs* NHE). Therefore, it is thermodynamically permissible for the transformation of the benzyl alcohol to the corresponding benzaldehyde by a direct photogenerated hole oxidation pathway under visible light irradiation; and the benzaldehyde cannot be further oxidized at the same conditions. Moreover, by carefully comparison of E_{CB} potential (−0.24 V *vs* NHE) and the oxidation potential of $O_2/{}^{\bullet}O_2^-$ (−0.33 V *vs* NHE), it was believed that M53/GR is incapable of the generation of ${}^{\bullet}O_2^-$ radicals by photo-induced electron reduction of molecular oxygen. So the pathway that the oxidation of benzyl alcohol into benzaldehyde by the ${}^{\bullet}O_2^-$ radicals cannot be occurred.

In Table 2, blank control and active species trapping experiments were carried out. The conversations of benzyl alcohol were nearly to 0 in the dark and without the photocatalyst (**Entries 1**

Table 2
Active species trapping experiments of the photocatalytic oxidation by the M53/GR.

Entry	Catalyst	Solvent	Con./%	Sel./%
1[a]	None	CCl_4	None	None
2	MIL-53	CCl_4	28	>99
3	GR	CCl_4	0	0
4	M53/GR	CCl_4	74	>99
5	M53/GR	CCl_4 (KI)	32	>99
6[b]	M53/GR	CCl_4	0	0
7	M53/GR	CCl_4 (AO)	28	>99

[a] benzyl alchool 0.3 mmol, M53/GR-8 15 mg, CCl_4 10 mL, 7 h, visible-light illumination under ambient conditions.
[b] all conditions of b were same as a, the only difference is without the illumination of light source.

and 6). So the self-photooxidation of benzyl alcohol and oxidation in the dark could be neglected. Besides, only with pure GR and MIL-53(Fe) as the catalyst the conversion were 0 and 28%, respectively, (**Entries 2 and 3**), which were lower than the M53/GR as the catalyst (**Entry 4**). These results indicated that MIL-53(Fe) has photocatalytic effect for alcohol oxidation reaction. At the same time, it also shows that the nanocomposites, M53/GR, has better catalytic activity than MIL-53(Fe), The most reasonable explanation about this result is that the photocatalytic efficiency is intimately related with the fate and transfer of photogenerated electrons and holes, moreover it is consistent with results of the PL and the electrochemical impedance spectra (EIS) Nyquist plot in the below. On the other hand, based on the active species trapping experiments, that is, when using ammonium oxalate (AO) and potassium chloride (KCl) [52] as quencher for photogenerated holes in the oxidation system, the conversion of benzyl alcohol decreased significantly, it could be further confirmed that the photocatalytic oxidation of benzyl alcohol to benzaldehyde is driven by the photogenerated holes (Table 2**, entries 5 and 7**).

From another point of view, the result of the electrochemical impedance spectra (EIS) Nyquist plot (Fig. 5d) has further clarified the intimate interfacial contact can well improve the charge carrier transfer. As shown in Fig. 5d, M53/GR-8 has smaller radius of curvature compared to that of MIL-53(Fe), indicating the more efficient charge separation over M53/GR-8 nanocomposite. It is confirmed that interfacial contact between the MIL-53(Fe) and GR indeed plays an important role in the improvement of photocatalytic performance.

Based on the above discussion, a possible mechanism for the photocatalytic oxidation of benzyl alcohol over M53/GR is proposed (Scheme 1). Under visible- light irradiation, M53/GR is excited, meanwhile photogenerated electrons and holes are generated. On the one hand, the photogenerated holes with strong oxidation capacity can oxidize the benzyl alcohol directly. On the other hand, owing to the presence of GR sheets, the photogenerated electrons transfer to the GR. It inhibits the recombination of photogenerated electron-hole pairs efficiently. Furthermore, the photogenerated electron was extincted by the CCl_4 which is acted as the electron scavenger to further reduce the recombination of photogenerated electron-hole pairs, thus the more photogenerated holes should be allowed to participate in the oxidation reaction. As a result, M53/GR nanocomposites show perfect photocatalytic activities and high selectivity of the aldehydes or ketones in the photocatalytic oxidation reactions.

3.4. Catalyst recyclability and stability

For applications of heterogeneous photocatalysis, it is important that the photocatalytic material is stable under the experimental conditions. The stability of M53/GR-8 nanocomposite was evaluated by performing the recycle experiments under same conditions. It was simply recovered by filtration, washing with anhydrous ethanol and deionized water. After drying in vacuum at 80 °C for 4 h, it was subsequently used for another batch of oxidation under identical conditions. As shown in Fig. 6a, no significant loss of photocatalytic activities was observed after four cycles, which indicates sufficient recyclability of M53/GR-8 for the photocatalytic oxidation of benzyl alcohol. Furthermore, XRD and FT-IR results of the recovered catalyst were unchanged compared with the fresh one (Fig. 6b and c). It is revealed that the structure of M53/GR-8 was maintained even after the four cycles of the reaction.

4. Conclusions

In conclusion, we have prepared a series of MIL-53(Fe)-based photocatalysts, M53/GR nanocomposites, with different weight addition ratios of GR via a one-pot hydrothermal method. It has been demonstrated that the as-obtained M53/GR nanocomposites have higher photocatalytic activity than the bare MIL-53, the reason is that existence of the GR would minimize the recombination of photogenerated electron-hole pairs, and prolong the lifetime of electron-hole pairs. Moreover, M53/GR can perform as visible light driven photocatalysts for the selective oxidation of benzyl alcohol and many of it's derives to the corresponding aldehydes or ketones by photogenerated hole oxidation process under ambient conditions with environmentally benign. Meanwhile, the catalyst can be recycled at least four times without loss of catalytic efficiency. Most significantly, high selectivity of the aldehydes or ketones (99%) were obtained by the direct hole oxidation process. It would be used as a potential and promising strategy for the selective oxidation of alcohols. Therefore, this study provides new physical insights for design and choosing novel visible light active MOFs based photocatalyst.

Acknowledgements

The research was financial supported by NSFC (21163016, 21563026), Gansu provincial Natural Science Foundation of China (1208RJZA287), and the Program for Changjiang Scholars and Innovative Research Team in University (IRT15R56). We also thank Key Laboratory of Eco-Environment-Related Polymer Materials (Northwest Normal University), Ministry of Education, for financial support.

References

[1] N. Stock, S. Biswas, Chem. Rev. 112 (2011) 933–969.
[2] H.C. Zhou, J.R. Long, O.M. Yaghi, Chem. Rev. 112 (2012) 673–674.
[3] A.U. Czaja, N. Trukhan, U. Müller, Chem. Soc. Rev. 38 (2009) 1284–1293.
[4] S. Kitagawa, Chem. Soc. Rev. 43 (2014) 5415–5418.
[5] T. Zhang, W. Lin, Chem. Soc. Rev. 43 (2014) 5982–5993.
[6] J.L. Rowsell, O.M. Yaghi, Microporous Mesoporous Mat. 73 (2004) 3–14.
[7] X. Kang, H. Liu, M. Hou, X. Sun, H. Han, T. Jiang, Z. Zhang, B. Han, Angew. Chem. Int. Ed. 128 (2016) 1092–1096.
[8] Y. Fu, D. Sun, Y. Chen, R. Huang, Z. Ding, X. Fu, Z. Li, Angew. Chem. Int. Ed. 51 (2012) 3364–3367.
[9] M. Alvaro, E. Carbonell, B. Ferrer, F.X. Llabres i Xamena, H. Garcia, Chem. Eur. J. 13 (2007) 5106–5112.
[10] W. Zhen, J. Ma, G. Lu, Appl. Catal. B: Environ. 190 (2016) 12–25.
[11] J.L. Wang, C. Wang, W. Lin, ACS Catal. 2 (2012) 2630–2640.
[12] C.Y. Lee, O.K. Farha, B.J. Hong, A.A. Sarjeant, S.T. Nguyen, J.T. Hupp, J. Am. Chem. Soc. 133 (2011) 15858–15861.
[13] H. Furukawa, F. Gaíndara, Y.B. Zhang, J. Jiang, W.L. Queen, M.R. Hudson, O.M. Yaghi, J. Am. Chem. Soc. 136 (2014) 4369–4381.
[14] D. Wang, R. Huang, W. Liu, D. Sun, Z. Li, ACS Catal. 4 (2014) 4254–4260.
[15] D. Sun, Y. Fu, W. Liu, L. Ye, D. Wang, L. Yang, X. Fu, Z. Li, J. Chem. Eur. 19 (2013) 14279–14285.
[16] L. Ai, C. Zhang, L. Li, J. Jiang, Appl. Catal. B: Environ. 148–149 (2014) 191–200.
[17] D. Sun, L. Ye, Z. Li, Appl. Catal. B: Environ. 164 (2015) 428–432.
[18] C. Wang, Z. Xie, K.E. de Krafft, W. Lin, J. Am. Chem. Soc. 133 (2011) 13445–13454.
[19] X. Lang, X. Chen, J. Zhao, Chem. Soc. Rev. 43 (2014) 473–486.

[20] R. Liang, L. Shen, F. Jing, N. Qin, L. Wu, ACS Appl. Mater. Interfaces 7 (2015) 9507–9515.
[21] S. Wang, X. Wang, Small 11 (26) (2015) 3097–3112.
[22] L. Sciortino, A. Alessi, F. Messina, G. Buscarino, F.M. Gelardi, J. Phys. Chem. C 119 (2015) 7826–7830.
[23] X. Xu, R. Cao, S. Jeong, J. Cho, Nano Lett. 12 (2012) 4988–4991.
[24] T. Loiseau, C. Serre, C. Huguenard, G. Fink, F. Taulelle, M. Henry, T. Bataille, G. Ferey, J. Chem. Eur. 10 (2004) 1373–1382.
[25] D. Cunha, M. Ben Yahia, S. Hall, S.R. Miller, H. Chevreau, E. Elkaïm, G. Maurin, P. Horcajada, C. Serre, Chem. Mater. 25 (2013) 2767–2776.
[26] F. Millange, N. Guillou, M.E. Medina, G.R. Feírey, A. Carlin-Sinclair, K.M. Golden, R.I. Walton, Chem. Mater. 22 (2010) 4237–4245.
[27] K. Novoselov, A.K. Geim, S. Morozov, D. Jiang, M. Katsnelson, I. Grigorieva, S. Dubonos, A. Firsov, Nature 438 (2005) 197–200.
[28] N. Zhang, Y. Zhang, X. Pan, M.Q. Yang, Y.J. Xu, J. Phys. Chem. C 116 (2012) 18023–18031.
[29] C. Lavorato, A. Primo, R. Molinari, H. Garcia, J. Chem. Eur. 20 (2014) 187–194.
[30] M. Zhu, P. Chen, M. Liu, J. Mater. Chem. 22 (2012) 21487–21494.
[31] C. Petit, T.J. Bandosz, Adv. Mater. 21 (2009) 4753–4757.
[32] Y. Wu, H. Luo, H. Wang, RSC Adv. 4 (2014) 40435–40438.
[33] R. Lin, L. Shen, Z. Ren, W. Wu, Y. Tan, H. Fu, J. Zhang, L. Wu, Chem. Commun. 50 (2014) 8533–8535.
[34] W.S. Hummers Jr., R.E. Offeman, J. Am. Chem. Soc. 80 (1958), 1339–1339.
[35] D.V. Kosynkin, A.L. Higginbotham, A. Sinitskii, J.R. Lomeda, A. Dimiev, B.K. Price, J.M. Tour, Nature 458 (2009) 872–876.
[36] M. Mahyari, Y. Bide, J.N. Gavgani, Appl. Catal. A: Gen. 517 (2016) 100–109.
[37] X. Xiao, J. Jiang, L. Zhang, Appl. Catal. B: Environ. 142–143 (2013) 487–493.
[38] C. Zhang, L. Ai, J. Jiang, Ind. Eng. Chem. Res. 54 (2015) 153–163.
[39] P. Horcajada, P. Llewellyn, P. Horcajada, G. Maurin, T. Devic, N. Rosenbach, S. Bourrelly, C. Serre, D. Vincent, S. Loera-Serna, Y. Filinchuk, J. Am. Chem. Soc. 131 (2009) 13002–13008.
[40] A. Banerjee, R. Gokhale, S. Bhatnagar, J. Jog, M. Bhardwaj, B. Lefez, B. Hannoyer, S. Ogale, J. Mater. Chem. 22 (2012) 19694–19699.
[41] M.Q. Yang, Y.J. Xu, J. Phys. Chem. C 117 (2013) 21724–21734.
[42] Z.H. Sheng, L. Shao, J.J. Chen, W.J. Bao, F.B. Wang, X.H. Xia, ACS Nano 5 (2011) 4350–4358.
[43] X. Jian, X. Liu, H.M. Yang, J.G. Li, X.L. Song, H.Y. Dai, Z.H. Liang, Appl. Surf. Sci. 370 (2016) 514–521.
[44] X. Huang, C. Tan, Z. Yin, H. Zhang, Adv. Mater. 26 (2014) 2185–2204.
[45] Z. Zhang, Y. Jiang, M. Chi, Z. Yang, G. Nie, X. Lu, C. Wang, Appl. Surf. Sci. 363 (2016) 578–585.
[46] R. Liang, F. Jing, L. Shen, N. Qin, L. Wu, J. Hazard. Mater. 287 (2015) 364–372.
[47] S. Sepúlveda Guzmán, L. Lara, O. Pérez Camacho, O. Rodríguez Fernández, A. Olivas, R. Escudero, Polymer 48 (2007) 720–727.
[48] G.T. Vuong, M.H. Pham, T.O. Do, Dalton Trans. 42 (2012) 550–557.
[49] W. Yue, S.L. Suraru, D. Bialas, M. Müller, F. Würthner, Angew. Chem. Int. Ed. 53 (2014) 6159–6162.
[50] L.P. Sun, S.Y. Niu, J. Jin, G.D. Yang, L. Ye, Inorg. Chem. Commun. 9 (2006) 679–682.
[51] X. Jin, L. Ye, H. Wang, Y. Su, H. Xie, Z. Zhong, H. Zhang, Appl. Catal. B: Environ. 165 (2015) 668–675.
[52] S. Li, D. Meng, L. Hou, D. Wang, T. Xie, Appl. Surf. Sci. 371 (2016) 164–171.